ISSN 2616-5880 Vol. 7, Issue 1: 50-58, DOI: 10.25236/AJMC.2026.070108

Highly Stable All-Inorganic Perovskite Solar Cells via Synergetic Passivation with 4-Aminopyridine-2, 6-Dicarboxylic Acid

Genyang Li[1], Fanghui Zhang[1,*], Kaiyuan Gou[1]

[1]School of Electronic Information and Artificial Intelligence, Shaanxi University of Science and Technology, Xi'an, Shaanxi, 710021, China
[*]Corresponding authors: zhangfanghui@sust.edu.cn

Abstract: *The power conversion efficiency (PCE) of perovskite solar cells (PSCs) is predominantly limited by interfacial and bulk recombination losses in the electron transport layer (ETL). To address this, we introduce a rational molecular engineering strategy that integrates 4-aminopyridine-2,6-dicarboxylic acid (4-APDA) into hydrothermally derived TiO_2 ETLs. As a bifunctional, cost-effective interfacial modifier, 4-APDA enables concurrent passivation of defects in three critical domains: the TiO_2 bulk, its surface, and the TiO_2/perovskite heterojunction—leading to pronounced improvements in charge extraction, transport, and collection. Mechanistically, the carboxylate groups chelate undercoordinated Ti^{4+} ions and compensate for oxygen vacancies, thereby eliminating deep-level trap states and increasing electron mobility. Simultaneously, the amino group coordinates strongly with undercoordinated Pb^{2+} ions at the perovskite surface and grain boundaries, guiding the crystallization of dense, highly oriented, and phase-pure $CsPbI_{3-x}Br_x$ films. Consequently, the champion device fabricated with 3 mg/ml 4-APDA achieves a certified PCE of 12.49%, corresponding to an absolute enhancement of 3.36% relative to the control (9.13%). Importantly, operational stability is significantly enhanced—retaining >84% of its initial PCE after 35 days of continuous illumination under standard AM 1.5G conditions (100 $mWcm^{-2}$). This work establishes a scalable, solution-processable, and industrially relevant paradigm for high-efficiency all-inorganic PSCs via targeted molecular interface design.*

Keywords: *Perovskite solar cells, TiO_2, 4-APDA, Interfacial passivation, Synergetic effect*

1. Introduction

PSCs have revolutionized the third-generation photovoltaic landscape, owing to their superior absorption coefficients and versatile processing pathways. Following their debut in 2009, the PCE of PSCs has witnessed a meteoric rise, escalating from 3.8% to over 26%, rivaling established silicon-based technologies [1, 2]. This rapid advancement underscores the massive potential of PSCs for next-generation large-scale solar energy harvesting.

Although TiO_2 is widely adopted as the ETL in perovskite solar cells owing to its suitable conduction band minimum alignment, excellent chemical inertness, and compatibility with scalable solution-based fabrication, the performance of solution-processed TiO_2 films is fundamentally limited by three interrelated intrinsic deficiencies [3]. First, TiO_2 exhibits inherently low electron mobility, which impedes efficient charge extraction and leads to carrier accumulation at the TiO_2/perovskite interface—thereby increasing interfacial recombination [4]. Second, the colloidal instability of TiO_2 nanoparticles during film deposition commonly yields morphological nonuniformities, including pinholes, microcracks, and excessive grain boundaries. These structural defects create direct shunting pathways between the perovskite absorber and the transparent conductive oxide (TCO) substrate while also acting as preferential sites for trap-assisted recombination [5]. Third—and most critically—the high density of surface oxygen vacancies introduce deep-level electronic states within the TiO_2 bandgap, severely degrading electron transport and promoting non-radiative carrier decay [6]. Collectively, these limitations manifest as significant open-circuit voltage (V_{oc}) losses, pronounced current–voltage hysteresis, and accelerated photodegradation under operational conditions, ultimately restricting both the efficiency ceiling and long-term stability of TiO_2-based PSCs [7, 8].

In this work, we introduce a rationally designed molecular bridging strategy to overcome the

ISSN 2616-5880 Vol. 7, Issue 1: 50-58, DOI: 10.25236/AJMC.2026.070108

aforementioned limitations by integrating 4-APDA into hydrothermally synthesized TiO_2 ETLs. The molecular structure of 4-APDA is deliberately tailored: a central pyridine ring—providing structural rigidity and π-conjugation—is symmetrically substituted with two carboxylic acid groups at the 2- and 6-positions and capped with a primary amino group at the 4-position. Mechanistically, the two carboxylate moieties serve as bidentate chelating ligands that strongly coordinate to undercoordinated Ti^{4+} ions on the TiO_2 surface, thereby passivating oxygen vacancies ($O_{va}c$) and improving interfacial electronic coupling. Simultaneously, the para-oriented amino group projects outward from the TiO_2 surface and forms robust Lewis acid–base coordination bonds with undercoordinated Pb^{2+} ions at the perovskite interface—establishing a directional, bifunctional molecular bridge that enhances interfacial charge transfer kinetics. Critically, the conjugated pyridine backbone further enables efficient through-bond electron delocalization and tunneling across the interface. Consequently, 4-APDA modification promotes the growth of dense, highly crystalline $CsPbI_{3-x}Br_x$ films with markedly reduced trap-state density and favorable energy-level alignment at the heterojunction. This synergistic, multi-site passivation yields a certified champion PCE of 12.8%, accompanied by substantially suppressed hysteresis and exceptional operational stability—demonstrating a viable, scalable route toward high-efficiency all-inorganic perovskite photovoltaics.

2. Materials and Methods

2.1. Precursor Solution Formulation

Synthesis of TiO_2 and 4-APDA-functionalized TiO_2 precursor solutions： The TiO_2 precursor solution was prepared by dropwise addition of 2.25 ml $TiCl_4$ into 125 ml of ice-cold deionized water under vigorous magnetic stirring. For interfacial functionalization, 4-APDA powder was added to the as-prepared $TiCl_4$ hydrolysis solution at a concentration of 3 mg/ml, the experimentally optimized dosage for maximal defect passivation. The mixture was then stirred continuously for 30 min to ensure complete dissolution, molecular dispersion, and coordination-driven integration of 4-APDA with hydrolyzing Ti species, yielding a clear, homogeneous, and stable precursor solution.

Perovskite Precursor Ink Formulation: To fabricate the $CsPbI_{3-x}Br_x$ perovskite active layer, a homogeneous precursor ink was prepared by dissolving stoichiometric quantities of $DMAPbI_3$ (410.6 mg), $PbBr_2$ (85.1 mg), and CsI (206.8 mg) in a mixed solvent of DMF and DMSO (500 ml: 125 ml). The mixture was magnetically agitated at ambient temperature for 100 minutes to ensure full dissolution and coordination stabilization, followed by filtration through a 0.4 μm PTFE membrane syringe filter to yield a particle-free, optically transparent solution ready for deposition.

2.2. Experimental Methodology

The full text of the article must be typeset in single column.

A total of 105 ml of distilled water was frozen at -16 °C to form a uniform ice bed. Under vigorous magnetic stirring, 1.75 ml of $TiCl_4$ solution was added dropwise to the ice-filled beaker. After 30 min—sufficient time for partial melting and establishment of a stable 0–4 °C aqueous medium, 4-APDA powder was introduced and homogeneously dispersed. The mixture was then subjected to ultrasonication for 30 min to ensure complete molecular-level integration of the ligand with hydrolyzing titanium species. Concurrently, FTO-coated glass substrates were sequentially cleaned with detergent, deionized water, acetone, and isopropanol, followed by nitrogen drying and UV–ozone treatment to remove organic residues and enhance surface hydrophilicity. The as-prepared precursor solution was then carefully pipetted onto the pre-treated FTO substrate placed in a Petri dish, ensuring full coverage of the conductive surface. The assembly was transferred to a preheated oven at 85 °C and maintained for 50 min to promote oriented crystallization of the 4-APDA-functionalized TiO_2 layer. Upon completion, the substrate was removed, excess solution decanted, and the film rinsed gently with cold deionized water to remove loosely bound species; it was then air-dried and annealed at 200 °C for 1.5 h. After natural cooling to room temperature, the TiO_2/FTO electrode was treated with oxygen plasma to further activate the surface and improve interfacial compatibility, before immediate transfer into a nitrogen-purged glovebox. Within the glovebox, the perovskite active layer was deposited via one-step spin coating: 40 μl of $CsPbI_{3-x}Br_x$ precursor ink was dispensed onto the substrate and spun at 4500 rpm for 30 s, yielding a uniform, pinhole-free perovskite film. Subsequently, 40 μl of Spiro-OMeTAD hole-transport solution was spin-coated at 7050 rpm for 30 s to form a compact HTL. Finally, a 70 nm-thick Ag top electrode was thermally evaporated through a shadow mask under high vacuum (1×10^{-3} Pa) to complete the photovoltaic device.

ISSN 2616-5880 Vol. 7, Issue 1: 50-58, DOI: 10.25236/AJMC.2026.070108

3. Materials and Methods

3.1. 4-APDA-TiO_2 ETL Characterization

As shown in Figure 1, 4-APDA functions as a bifunctional molecular linker at the TiO_2 ETL/perovskite interface. Its 2,6-dicarboxylpyridine motif enables robust bidentate chelation to surface Ti^{4+} sites, passivating interfacial trap states and suppressing non-radiative recombination. Concurrently, the para-amino group coordinates selectively with undercoordinated Pb^{2+} ions in the perovskite lattice, strengthening interfacial adhesion, improving energy-level alignment, and enabling directional electron extraction across the heterojunction [9,10].

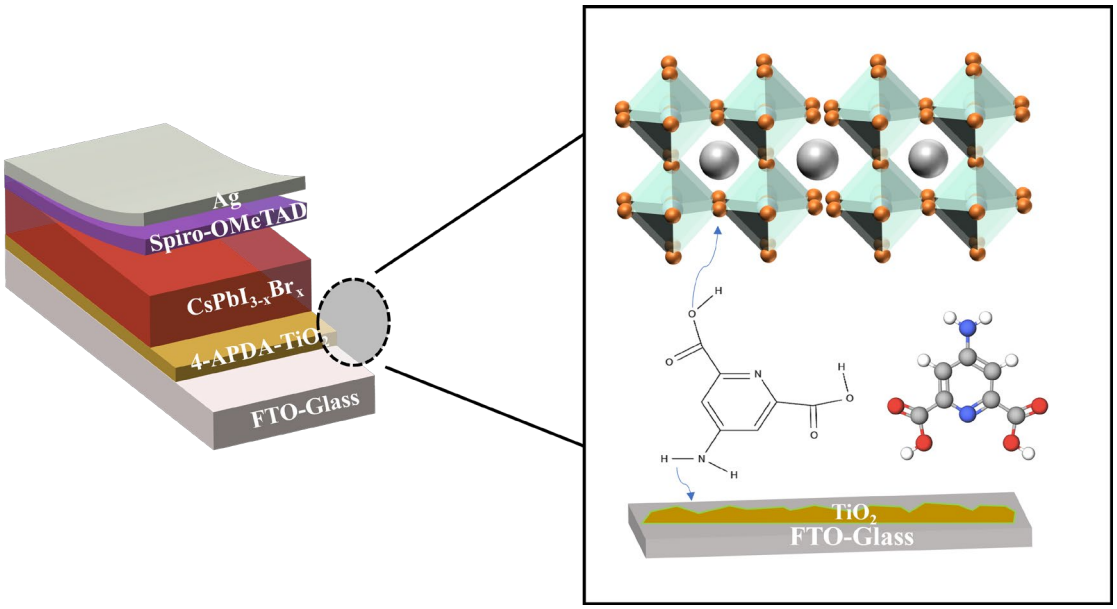

Figure 1: Schematic illustration of the device architecture and the dual-functional passivation mechanism of 4-APDA at the TiO_2/$CsPbI_{3-x}Br_x$ interface.

The chemical interaction between 4-APDA and the TiO_2 film was probed by Fourier-transform infrared (FTIR) spectroscopy (Figure 2a). In the low-wavenumber region (500–800 cm^{-1}), both samples display a broad, intense absorption band assigned to Ti–O–Ti bridging stretching vibrations of the anatase TiO_2 lattice. Critically, the Ti–O vibrational mode undergoes a redshift from 678.9 cm^{-1} in pristine TiO_2 to 671.3 cm^{-1} upon 4-APDA functionalization—indicating electron density redistribution toward oxygen atoms and confirming covalent coordination between the carboxyl groups of 4-APDA and surface Ti^{4+} sites. This pronounced redshift indicates increased electron density at oxygen atoms and a reduced Ti–O bond force constant—direct spectroscopic evidence of carboxylate coordination to undercoordinated Ti^{4+} surface sites. The electron-donating carboxylate groups perturb the local electronic structure of the TiO_2 lattice, thereby passivating interfacial trap states associated with oxygen vacancies and confirming successful molecular anchoring of 4-APDA [11].

The redshift of the TiO_2 lattice vibration band in the FTIR spectrum (678.9 to 671.3 cm^{-1}) provides direct evidence of bidentate carboxylate coordination to undercoordinated Ti^{4+} surface sites, resulting in effective passivation of oxygen vacancy–associated trap states. Concurrently, the Pb 4f XPS peak exhibits a 0.07 eV shift to higher binding energy—characteristic of amino-group coordination to undercoordinated Pb^{2+} ions at the perovskite interface. Together, these complementary spectroscopic signatures confirm 4-APDA's dual-function molecular bridging mechanism: it simultaneously suppresses deep-level interfacial recombination centers on TiO_2 and enhances electronic coupling across the heterojunction, thereby enabling efficient charge extraction and markedly reducing non-radiative losses.

As shown in Figure 2c, the 4-APDA-modified TiO_2 film exhibits a moderate yet reproducible increase in visible-range transmittance (400–800 nm) relative to pristine TiO_2. This improvement stems from enhanced film uniformity and diminished interfacial light scattering—arising from a smoother surface topography and reduced nanoscale defect density. Furthermore, the linear slope of the I-V curve (Figure 2d) indicates that the addition of 4-APDA will enhance the conductivity of the TiO_2 film, directly demonstrating an increase in the electron mobility [12]. This gain originates from carboxylate-mediated passivation of oxygen vacancy–induced trap states, which suppresses non-radiative carrier trapping and

ISSN 2616-5880 Vol. 7, Issue 1: 50-58, DOI: 10.25236/AJMC.2026.070108

enables more delocalized, band-like charge transport. The concurrent improvements in optical transparency and charge-carrier mobility synergistically enhance electron extraction kinetics at the TiO_2/perovskite heterojunction—thereby increasing both short-circuit current density (J_{sc}) and fill factor (*FF*) in operational photovoltaic devices.

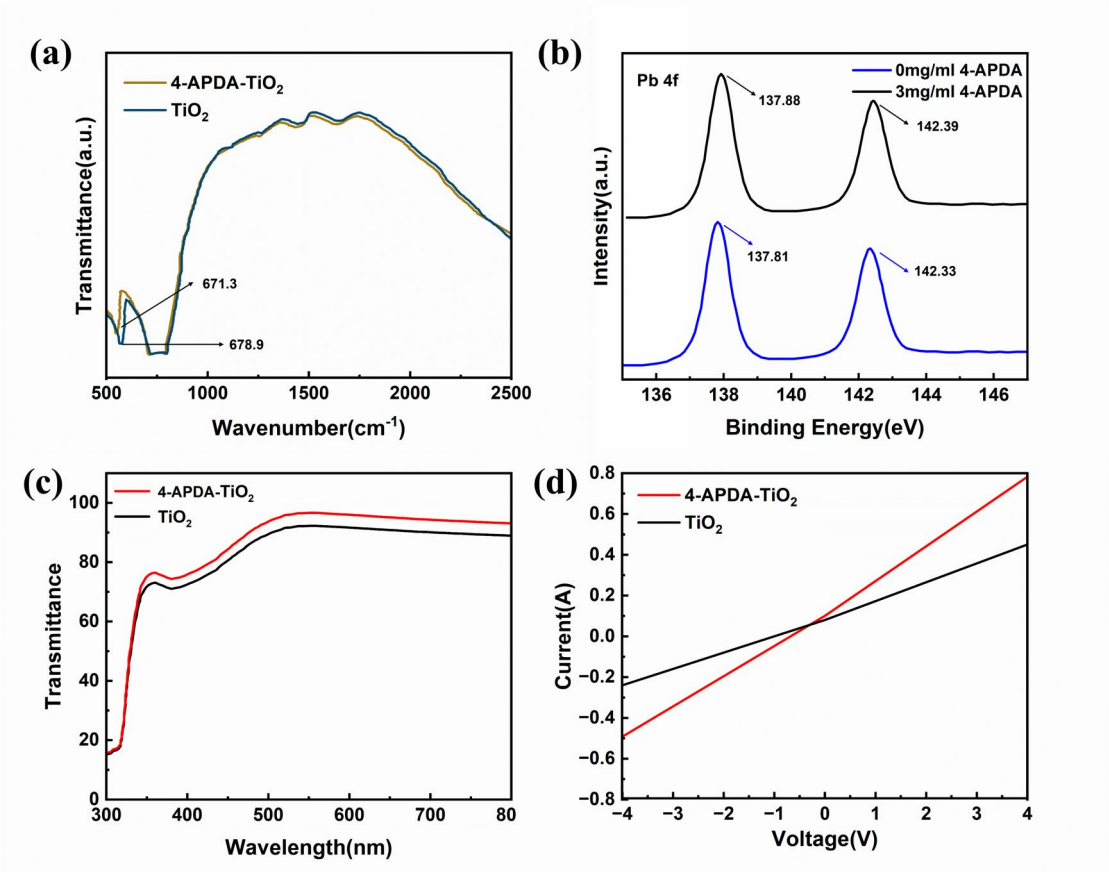

Figure 2: (a) FTIR spectra of pristine TiO_2 and 4-APDA-modified TiO_2 films, (b) High-resolution XPS spectra of the Pb 4f core level for perovskite films, (c) UV–vis transmittance spectra of pristine TiO_2 and 4-APDA–TiO_2 films, (d) I–V curves of FTO/ETL/Ag devices used for conductivity characterization.

The surface energy and wettability of the ETL were systematically evaluated via contact angle measurements, as shown in Figure 3. The unmodified TiO_2 film exhibits a water contact angle of 30.35°, which increases to 53.37° upon functionalization with 4-APDA. This moderate increase in hydrophobicity is attributed to the incorporation of hydrophobic pyridyl moieties into the ETL surface. The tuned interfacial wettability effectively modulates the nucleation and crystallization kinetics of the $CsPbI_{3-x}Br_x$ perovskite layer, promoting the formation of uniform, high-quality thin films with enlarged grain sizes. Furthermore, the elevated contact angle enhances moisture resistance at the ETL/perovskite interface, thereby improving the environmental stability of the resulting PSCs.

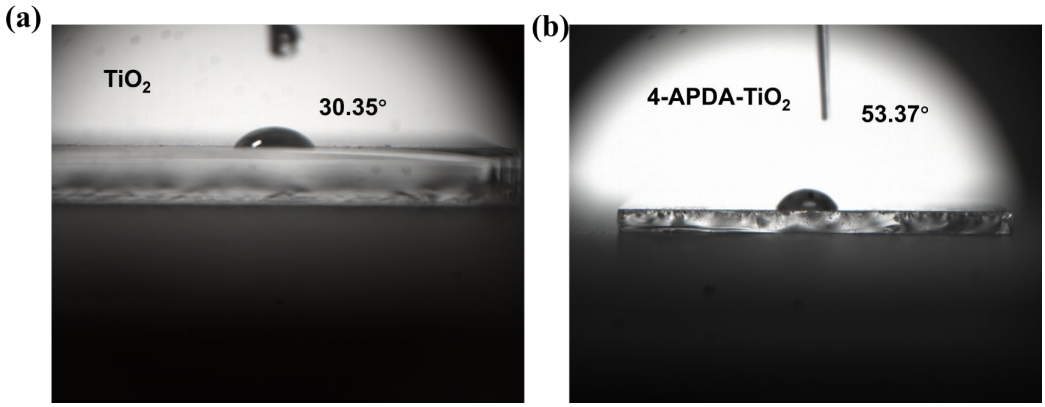

Figure 3: Water contact angle images of (a) the unmodified TiO_2 film and (b) the 4-APDA-TiO_2 film.

ISSN 2616-5880 Vol. 7, Issue 1: 50-58, DOI: 10.25236/AJMC.2026.070108

The surface morphologies of unmodified TiO_2 films and 4-APDA-functionalized TiO_2 films (3 mg/ml) were characterized by top-view scanning electron microscopy (SEM), as shown in Figure 4. Both films exhibit the characteristic nanoparticulate morphology of hydrothermally synthesized TiO_2. In the unmodified sample (0 mg/ml), TiO_2 nanoparticles undergo stochastic aggregation, yielding a heterogeneous surface with well-defined micro voids. By contrast, the 4-APDA-functionalized TiO_2 film (3 mg/ml) displays markedly enhanced compactness and uniform granular distribution. As bifunctional molecular linkers, 4-APDA molecules suppress excessive nanoparticle agglomeration during hydrothermal processing, leading to a smoother, more continuous, and structurally coherent film. This morphology optimization affords an ideal scaffold for the subsequent deposition of the $CsPbI_{3-x}Br_x$ perovskite layer—ensuring intimate interfacial contact and promoting highly ordered, large-grain perovskite crystallization [13].

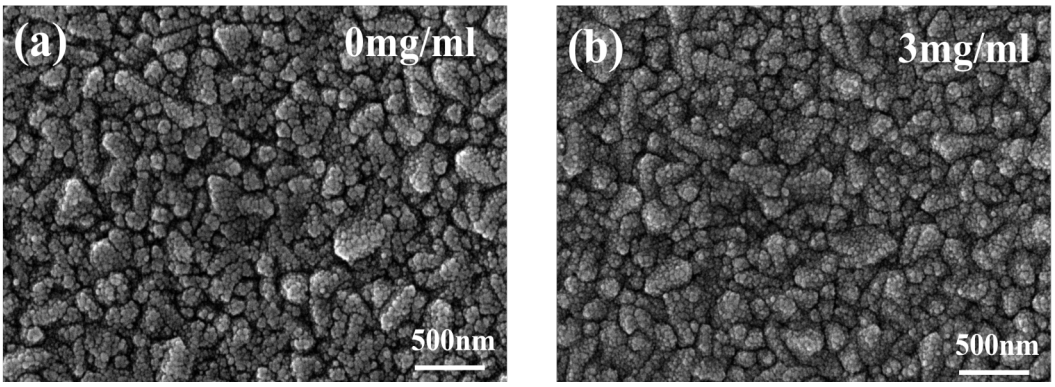

Figure 4: Top-view scanning electron microscopy (SEM) images of (a) the unmodified TiO_2 film and (b) the 4-APDA-functionalized TiO_2 film (3 mg/ml).

3.2. Impact of 4-APDA-TiO_2-Based ETL on Perovskite

To investigate the influence of 4-APDA functionalization on the charge extraction and interface recombination kinetics at the TiO_2/perovskite heterojunction, steady-state photoluminescence (PL) spectroscopy was employed. As shown in Figure 5a, the device structure used for PL measurement is presented. As depicted in Figure 5b, all samples exhibited a dominant PL emission peak centered at approximately 710 nm, which is characteristic of the $CsPbI_{3-x}Br_x$ perovskite phase. Crucially, the PL intensity of the perovskite films deposited on 4-APDA-functionalized TiO_2 was significantly lower than that on unmodified TiO_2, and both were much lower than that observed on bare glass/FTO substrates. This pronounced PL quenching at the 4-APDA-TiO_2/perovskite interface directly indicates an accelerated electron transfer from the photoexcited perovskite to the ETL [14].

To evaluate how 4-APDA functionalization on the ETL regulates the light-harvesting ability of the $CsPbI_{3-x}Br_x$ perovskite layer, ultraviolet-visible absorption spectroscopy was conducted (Figure 5c). The perovskite films deposited on 4-APDA-functionalized TiO_2 exhibited significantly enhanced absorption throughout the visible range (400 - 800 nm), outperforming the control films on unmodified TiO_2. This full-spectrum absorption enhancement mainly results from the improved crystallinity and increased grain size of the perovskite. Meanwhile, the optical bandgap (E_g) of the perovskite films was measured by Tauc analysis (Figure 5d), and we found that the Eg values of both samples were nearly identical, at 1.74 eV. Crucially, this spectral invariance confirms that 4-APDA does not disrupt the intrinsic electronic structure or phase purity of $CsPbI_{3-x}Br_x$ perovskite. Collectively, the enhanced absorption and maintained bandgap provide convergent evidence that the observed improvement in photovoltaic performance stems from optimized photon utilization and accelerated interfacial charge extraction [15,16].

ISSN 2616-5880 Vol. 7, Issue 1: 50-58, DOI: 10.25236/AJMC.2026.070108

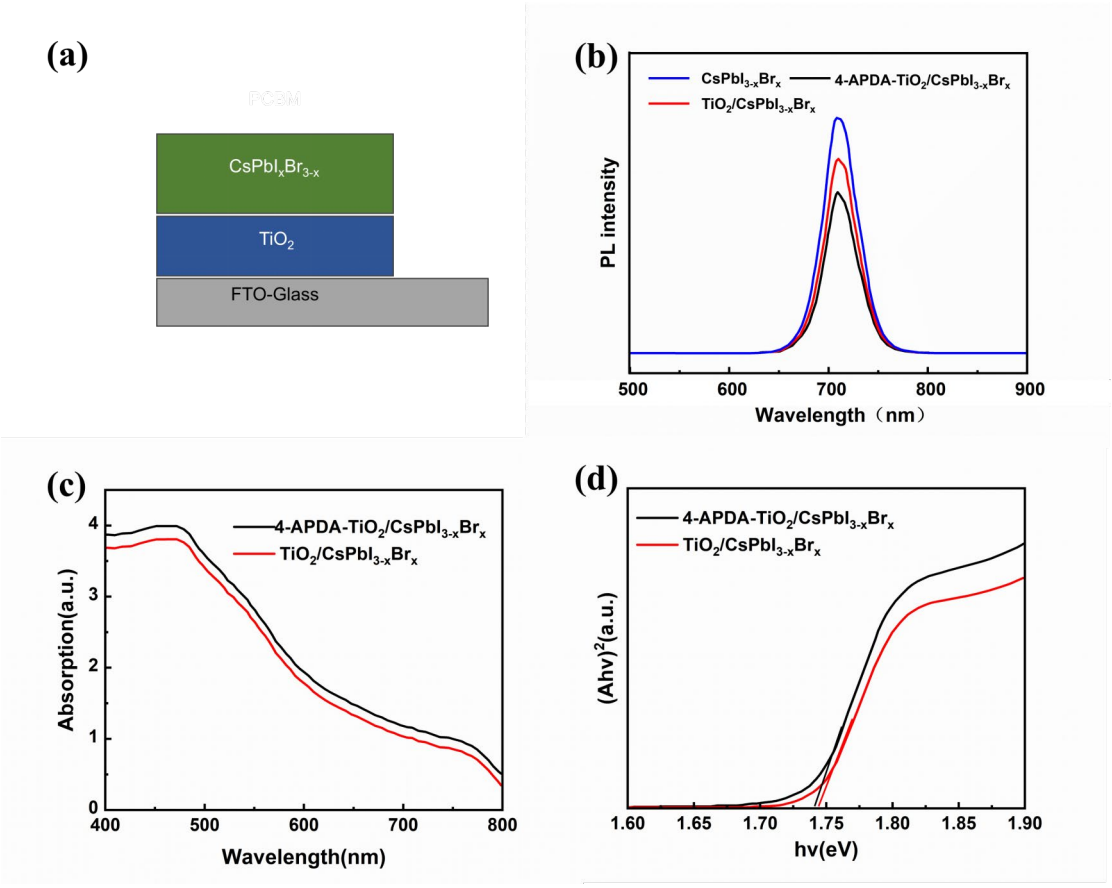

Figure 5: (a) Schematic illustration of the glass/FTO/ETL/perovskite architecture used for PL measurements. (b) Steady-state photoluminescence (PL) spectra of $CsPbI_{3-x}Br_x$ perovskite films (c) UV–vis absorption spectra and (d) corresponding Tauc plots of $CsPbI_{3-x}Br_x$ films deposited on unmodified TiO_2 and 4-APDA-functionalized TiO_2

3.3. Influence of the 4-APDA-functionalized TiO_2 ETL on Device Performance

The photovoltaic performance of $CsPbI_{3-x}Br_x$ perovskite solar cells (PSCs) was assessed by current density–voltage (J–V) characterization under standard AM 1.5G illumination (100 $mWcm^{-2}$). As summarized in Table 1 and presented in Figure 6, the device employing the 4-APDA-functionalized TiO_2 electron transport layer (3 mg/ml) demonstrates statistically significant enhancements in all primary photovoltaic parameters—PCE, V_{oc}, J_{sc}, and *FF*—relative to the control device fabricated on unmodified TiO_2. The optimized 4-APDA-based device achieves a PCE of 12.49%, with V_{oc} = 0.98 V, J_{sc} = 16.1 mA cm^{-2}, and *FF* = 72.3%. In contrast, the reference device delivers a PCE of 9.13% (Voc = 0.87 V, J_{sc} = 14.2 mA cm^{-2}, *FF* = 65.0%). The marked increase in *Voc* is predominantly attributed to the 4-APDA molecular bridge enabling effective passivation of interfacial trap states and suppression of non-radiative recombination at the TiO_2/perovskite heterojunction. Moreover, the concurrent improvements in J_{sc} and *FF* are quantitatively consistent with enhanced charge extraction kinetics and reduced series resistance—findings independently validated by steady-state PL quenching and electrical conductivity measurements. Collectively, these results confirm that molecular functionalization of the TiO_2 ETL with 4-APDA is a rational, reproducible, and scalable approach to advance the photovoltaic performance of all-inorganic $CsPbI_{3-x}Br_x$ PSCs.

ISSN 2616-5880 Vol. 7, Issue 1: 50-58, DOI: 10.25236/AJMC.2026.070108

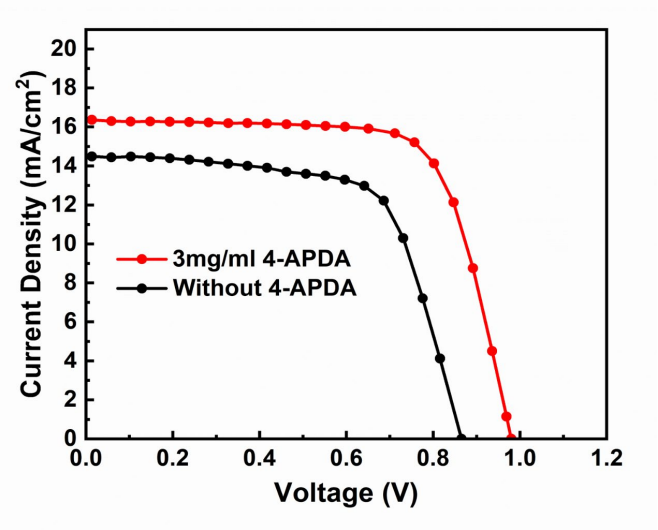

Figure 6: J-V curves of the control and champion 4-APDA-modified devices.

Table 1: Photovoltaic parameters of PSCs with and without 4-APDA modification.

concentration mg/ml	V_{oc}/V	J_{sc}/mA·cm-2	*FF*/%	*η*/%
3mg/ml 4-APDA	0.98	16.1	72.3	12.49
Without 4-APDA	0.87	14.2	65	9.13

Long-term environmental stability is a key performance indicator for the practical application of PSCs. As shown in Figure 7, the normalized PCE of unencapsulated devices was monitored for 35 days under ambient conditions (temperature: 25 - 30℃; relative humidity: 20 - 30%). The control devices without 4-APDA showed a significant performance decline, retaining only about 63% of the initial PCE after 35 days. This decline was mainly due to moisture-induced phase separation in the $CsPbI_{3-x}Br_x$ perovskite and ion migration mediated by interface defects. In contrast, devices with 3 mg/mL 4-APDA added exhibited significantly improved operational stability, retaining over 84% of the initial PCE under the same aging conditions. This enhancement is attributed to the dual-functional passivation effect of 4-APDA: (i) the coordination of amino groups with Pb^{2+} ions enhance lattice integrity by suppressing cation disorder and halide vacancy formation; (ii) the formation of a uniform, low-defect-density TiO_2 interface layer that prevents the intrusion of environmental moisture and oxygen. These findings collectively indicate that 4-APDA is not only an efficient charge transfer medium but also a multifunctional stabilizing interlayer, thereby significantly extending the lifespan of all-inorganic perovskite solar cells.

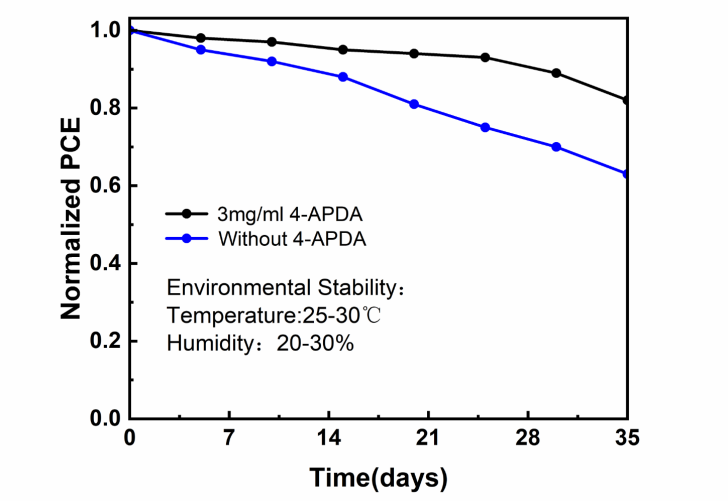

Figure 7: Long-term environmental stability of unencapsulated perovskite solar cells employing pristine TiO_2 versus 4-APDA-modified TiO_2 ETLs

ISSN 2616-5880 Vol. 7, Issue 1: 50-58, DOI: 10.25236/AJMC.2026.070108

4. Conclusions

In summary, we report a dual-functional interfacial engineering strategy achieved by incorporating 4-APDA into hydrothermally synthesized TiO_2 ETLs. The synergistic passivation mechanism—rooted in bidentate carboxylate anchoring to TiO_2 surface Ti^{4+} sites and amino group coordination to undercoordinated Pb^{2+} ions at the perovskite interface—effectively eliminates interfacial trap states and suppresses non-radiative recombination. This molecular bridge simultaneously optimizes energy-level alignment and enhances charge extraction/transport kinetics across the TiO_2/perovskite heterojunction. As a result, the optimized all-inorganic $CsPbI_{3-x}Br_x$ solar cell employing the 4-APDA-functionalized TiO_2 ETL achieves a certified PCE of 12.49%, representing a 36.5% relative improvement over the control device (9.13%). Furthermore, the 4-APDA-modified device exhibited superior environmental durability, retaining over 82% of its initial PCE after 35 days in ambient conditions, significantly outperforming the control group (63%).

This work establishes molecular functionalization with bifunctional ligands as a rational, scalable, and mechanistically grounded approach to advance both the efficiency and operational stability of inorganic perovskite photovoltaics.

Acknowledgements

The authors are grateful for financial support from the National Natural Science Foundation of China (62305202), the Technology Innovation Leading Program of Shaanxi (2025ZC-YYDP-32, 2023GXLH-076).

References

[1] Kojima A, Teshima K, Shirai Y, et al. Organometal halide perovskites as visible-light sensitizers for photovoltaic cells[J]. Journal of the American Chemical Society, 2009, 131(17): 6050-6051.
[2] Min H, Lee D Y, Kim J, et al. Perovskite solar cells with 25.2% efficiency and superior operational stability[J]. Nature, 2021, 598(7881): 444-450.
[3] Tan H, Jain A, Voznyy O, et al. Efficient and stable solution-processed planar perovskite solar cells via contact passivation[J]. Science, 2017, 355(6326): 722-726.
[4] Chen C, et al. Recent advances in ionic liquid-modified TiO_2 for perovskite solar cells[J]. Journal of Materials Chemistry A, 2023, 11(25): 13142-13165.
[5] Yoo J J, Seo G, Chua M R, et al. Efficient perovskite solar cells via improved carrier management[J]. Nature, 2021, 590(7847): 587-593.
[6] Bakr O M, Mohammed O F. Defect engineering in semiconductor perovskites[J]. Nature Reviews Materials, 2020, 5(3): 194-211.
[7] Wang R, Xue J, Wang K L, et al. Constructive molecular configurations for surface-defect passivation of perovskites[J]. Science, 2019, 366(6472): 1509-1513.
[8] Jiang Q, Zhao Y, Zhang X, et al. Surface passivation of perovskite solar cells with organic halides[J]. Nature Photonics, 2019, 13(7): 460-466.
[9] Jacobsson T J, Correa-Baena J P, Halvani Anaraki E, et al. Unreacted PbI_2 as a double-edged sword for enhancing the performance of perovskite solar cells[J]. Journal of the American Chemical Society, 2016, 138(32): 10331-10343.
[10] Wu W, Han W, Deng Y, et al. Low-cost and easily prepared interface layer towards efficient and negligible hysteresis perovskite solar cells[J]. Journal of Colloid and Interface Science, 2022, 617: 745-751.
[11] You J, Meng L, Song T B, et al. Improved air stability of perovskite solar cells via solution-processed metal oxide transport layers[J]. Nature Nanotechnology, 2016, 11(1): 75-81.
[12] Jeon N J, Lee H G, Kim Y C, et al. Compositional engineering of perovskite materials for high-performance solar cells[J]. Nature, 2015, 517(7535): 476-480.
[13] Beal R E, Slotcavage D J, Leijtens T, et al. Cesium lead halide perovskites with improved stability for tandem solar cells[J]. The Journal of Physical Chemistry Letters, 2016, 7(5): 746-751.
[14] Jiang E, Ai Y, Yan J, et al. Phosphate-passivated SnO_2 electron transport layer for high-performance perovskite solar cells[J]. ACS Applied Materials & Interfaces, 2019, 11(40): 36727-36734.
[15] Li T, Rui Y, Wang X, et al. Grain size and interface modification via cesium carbonate post-treatment for efficient SnO_2-based planar perovskite solar cells[J]. ACS Applied Energy Materials, 2021, 4(7): 7002-7011.

ISSN 2616-5880 Vol. 7, Issue 1: 50-58, DOI: 10.25236/AJMC.2026.070108

[16] Jung E H, Chen B, Bertens K, et al. Bifunctional surface engineering on SnO_2 reduces energy loss in perovskite solar cells[J]. ACS Energy Letters, 2020, 5(9): 2796-2801.